


Ab initio investigation of the role of charge transfer in the adsorption properties of H₂, N₂, O₂, CO, NO, CO₂, NO₂, and CH₄ on the van der Waals layered Sn₃O₄ semiconductorRafael L. H. Freire^{1,*}, Marcelo O. Orlandi^{2,†} and Juarez L. F. Da Silva^{3,‡}¹Beijing Computational Science Research Center, Beijing 100193, People's Republic of China²Department of Engineering, Physics and Mathematics, São Paulo State University (UNESP), 14800-060, Araraquara, SP, Brazil³São Carlos Institute of Chemistry, University of São Paulo, P.O. Box 780, 13560-970, São Carlos, SP, Brazil (Received 5 July 2020; revised 29 August 2020; accepted 15 September 2020; published 2 October 2020)

We report an atomistic investigation, based on density functional theory calculations within the D3 van der Waals correction, of the adsorption properties of H₂, N₂, O₂, CO, NO, CO₂, NO₂, and CH₄ on the semiconductor Sn₃O₄(010) monolayer surface. Except for NO₂ and NO molecules, the adsorption energies are from −64 meV (H₂) up to −167 meV (CO₂) with the molecule-surface distances larger than 3.30 Å for all molecules, and hence, minor effects were observed on the Sn₃O₄(010) surface electronic structure upon adsorption. NO₂ has the largest adsorption energy (−525 meV), which can be explained by closer approach of the two O atoms towards the surface, while NO binds to the surface with about half of the NO₂ adsorption energy (e.g., −279 meV). From Bader analysis, we found substantial charge transfer from the surface to the molecules, −0.52 *e* (NO₂) and −0.23 *e* (NO), which is consistent with the smaller distances to the surface, 2.46 and 2.82 Å, respectively. Thus, those results suggest an improved detection performance of Sn₃O₄ towards NO₂, which can help to design sensor devices based on the Sn₃O₄(010) monolayers.

DOI: [10.1103/PhysRevMaterials.4.104002](https://doi.org/10.1103/PhysRevMaterials.4.104002)**I. INTRODUCTION**

Two-dimensional (2D) van der Waals (vdW) layered solids have been employed in several applications [1–4], encompassing support for transition-metal (TM) particles in catalysis [5], electrodes candidates for energy storage [6,7], gas-sensor devices [8,9], etc. All those applications require a deep atomistic understanding of the adsorption properties of chemical species on solid surfaces. In such systems, the magnitude of the adsorption energy and electron transfer play a crucial role in several mechanisms such as the activation of CO₂, [10] substrate work function change employed as descriptor in gas-sensor devices, [11,12] etc.

In semiconductors and metal surfaces, the surface is obtained by cleaving the solid, which yields surfaces with dangling bonds, steps, kinks, etc. In contrast, the 2D vdW solids can yield well defined and relatively stable surfaces by an exfoliation process. Furthermore, single monolayers (MLs) derived from 2D vdW solids have higher energetic stability due to strong covalent and ionic bonds in-plane, and their weak vdW interactions with adsorbed molecules or supported particles and MLs [12]. Hence, our common atomistic understanding of molecular species adsorbed on metal or oxide surfaces cannot be easily transferred to those vdW surfaces. Thus, further studies are necessary to improve our under-

standing of vdW surfaces. Here, we will explore the Sn₃O₄ semiconductor [13,14], which forms special vdW structures among the SnO_{*n*} compounds [15–17], and has great potential for several applications.

The SnO_{*n*} (*n* = 1, $\frac{4}{3}$, 2) compounds have played an important role for several applications, e.g., gas sensor [18,19], photocatalytic water splitting [20], degradation of organic wastewater [21,22], monitoring of greenhouse gases [23], etc. For instance, SnO₂ is one of the most used material for gas sensor devices due to its high sensor response [19,24], which can be attributed to its high thermodynamic stability [25], energy band gap of 3.6 eV [26], and large concentration of oxygen vacancies [24], which helps to yield a *n*-type conductivity [15,24,27]. Furthermore, at its surface, there are cations species in the Sn²⁺ and Sn⁴⁺ oxidation states, which contributes to change the oxygen surface composition and its response properties [24].

On the other hand, alternative Sn–O compositions have been demonstrated to occur as a 2D layered vdW materials, like SnO and Sn₃O₄ [16,17,28], and could open new opportunities for applications. Compared to SnO₂, SnO has a smaller energy band gap, *E_g*, e.g., *E_g* = 2.7 (direct) and 0.70 eV (indirect) [29,30], and it is a *p*-type semiconductor at standard growth conditions [25,27,31–35]. Recently, Singh *et al.* have experimentally demonstrated the exfoliation of SnO microspheres into nanosheets of about 10 layers by sonication experiment [28]. Besides, Yao *et al.* employed density functional theory (DFT) calculations to study the adsorption properties of different molecules on the SnO surfaces. Among all studied molecules, NO, NO₂, and O₂ have the higher adsorption energies, which can affect the surface properties such as the work function. In addition, as a result of its smaller

*Present address: São Paulo State University Department of Engineering, Physics and Mathematics, São Paulo State University, 14800-060, Araraquara, SP, Brazil; freire.rafaelheleno@csrc.ac.cn

†marcelo.orlandi@unesp.br

‡juarez_dasilva@iqsc.usp.br

energy band gap (0.7 eV), it has been demonstrated that SnO could present *n*-type conduction through Sb doping or oxygen deficient synthesis, which make it suitable for transparent bipolar semiconductors [32,36].

In contrast to SnO₂ and SnO, which have been widely studied [19,24,31,32,36,37], Sn₃O₄ has not been well explored by experimental techniques or in adsorption studies. Particularly, its synthesis has been a challenging [38–41], which is attributed to its phase instability at temperatures above 600 °C as it starts to disproportionate into SnO₂ and metallic Sn [31,42,43]. Despite of that, in controlled O₂-atmosphere environment by a carbothermal reduction process, the Sn₃O₄ can be formed in O₂-deficient regime. Through optical measurements, Sn₃O₄ is known as an *n*-type semiconductor with experimental band gaps ranging from 2.4 to 2.9 eV [20,40,44].

While most of Sn₃O₄ applications comprises gas sensors devices, our knowledge about its properties still scarce and the atomistic understanding of the adsorption properties of molecules on the vdW Sn₃O₄ surface is far from satisfactorily, limiting its applications in different fields. For instance, Sn₃O₄ nanobelts (NBs) have demonstrated an enhanced sensor response for NO₂ [19], while Li *et al.* used a hydrothermal route to produce Sn₃O₄ nanoflowers, which showed an enhanced sensor response for ethanol compared to traditional tin oxides [45].

From theoretical results, it has been known that Sn₃O₄, as others intermediate tin oxides and SnO, presents a layered structure [29,34,46]. Wang *et al.* [16] demonstrated the need to consider van der Waals (vdW) interactions to describe the electronic and structural properties of intermediate tin oxides, firstly demonstrated to the SnO case [29]. In a previous work [47], by combining DFT and Dual Beam Microscopy (FIB-SEM), we have shown that the magnitude of the layer-layer interaction of Sn₃O₄ along its stacking direction [010] relies on the range of vdW layered materials. Moreover, by FIB-SEM, we have exfoliated a single Sn₃O₄ nanobelt, qualitatively endorsing a vdW layered structure, paving the way for new applications as a 2D material. Using a different approach, which is worth to notice, Wang *et al.* theoretically studied the electronic structure, as well as, some defect properties of mixed valence tin oxides, including Sn₃O₄ [16].

Thus, at this work, we aim to obtain an atomistic understanding of the adsorption properties of several molecules, namely, H₂, O₂, N₂, CO, NO, CO₂, NO₂, and CH₄, on the Sn₃O₄ ML through an *ab initio* approach based on DFT calculations within the additive vdW pairwise corrections as proposed by Grimme (D3) [48]. We found that, in general, the interactions molecule-surface are weak with adsorption energies <200 meV and, thus, minor impacts from the adsorbed species on the surface electronic structure. On the other hand, it is worth noticing that the interactions of O₂, NO, and NO₂ were relatively stronger, which can be explained by larger charge transfer based on the Bader analysis, $-0.12 e$, $-0.23 e$, and $-0.52 e$, respectively. Such effects contributed to the formation of an electron depletion region near to the vdW surface, then possibly increasing the monolayer resistance at experimental conditions. Particular attention should be given to NO₂ adsorption, once it was the most affecting molecule upon adsorption, with adsorption energy of about 500 meV and the smallest molecule-surface distance (2.46 Å). Thus

Sn₃O₄ monolayer seems to have an enhanced performance towards NO₂ detection [19,49], which is an important result for future applications employing this material.

II. THEORETICAL APPROACH AND COMPUTATIONAL DETAILS

All total energy calculations were based on spin-polarized DFT [50,51] within the generalized gradient approximation (GGA) exchange-correlation functional proposed by Perdew–Burke–Ernzerhof (PBE) [52]. To improve the description of the long-range vdW interactions, which can play a critical role for the weak interaction of molecules adsorbed on solid surfaces [53–57], we employed the pairwise D3 correction proposed by Grimme [58–60], as implemented in the Vienna *ab initio* simulation package (VASP) [61,62], in which an additive vdW energy correction is added to the DFT total energy [60,63]. In contrast with the vdW D2 correction [48], the vdW D3 correction accounts for interactions beyond the two-body terms [58,59,64], however, several studies have found that the three-body or Axilrod–Teller–Muto [65,66] terms play a major role only for large molecules [60,67], and hence, the energy contribution from the three-body terms are not added to the vdW D3 correction using IVDW = 11, in VASP. Thus, for a cross-check, we activate the three-body terms in VASP by changing an internal flag, and the addition of three-body term adds a contribution that raises the total energy of the adsorbed systems by about 0.21–0.23 eV, except for molecules in the gas-phase in which the three-body term is null. However, the changes in the adsorption energies are small, in general, they are reduced by less than 10 meV, except for NO₂ with 12.5 meV reduction, while there are no changes in the adsorption configuration geometry. Thus we employed the vdW D3 correction as implemented in VASP, i.e., without the three-body terms.

The total energies were obtained by the electron-ion core interactions described by the projector augmented wave (PAW) method [68,69], as implemented in VASP [61,62], version 5.4.1. The valence electrons were described by the scalar-relativistic approximation, where the spin-orbit coupling was not considered for the valence states. For all calculations, the cutoff energy for the plane-wave expansion of the Kohn–Sham orbitals was set to 466.5 eV, which is 12.5% larger than the recommended cutoff energy for O, while to obtain the equilibrium volume of the bulk system (triclinic unit cell) through the optimization of the stress tensor and atomic forces, we employed a cutoff energy of 622 eV due to the slower convergence of the stress tensor as a function of the number of plane waves.

Our bulk layered triclinic unit cell for Sn₃O₄ has the following DFT lattice parameters [47], $a_0 = 5.85 \text{ \AA}$, $b_0 = 8.18 \text{ \AA}$, and $c_0 = 4.91 \text{ \AA}$, Fig. 1. The Sn₃O₄(010) surface was modeled using a repeated slab model geometry composed by a 2×2 surface unit cell ($a = 9.82 \text{ \AA}$, $b = 11.69 \text{ \AA}$), a single Sn₃O₄ ML composed by 24 Sn and 32 O atoms, and a vacuum region of 16 Å. The Sn₃O₄ ML was placed at the bottom of the supercell, and the molecules were adsorbed only in one side of the slab, and hence, there is no inversion symmetry and dipole correction was taken into account. We will consider the adsorption of molecules on a clean monolayer, which

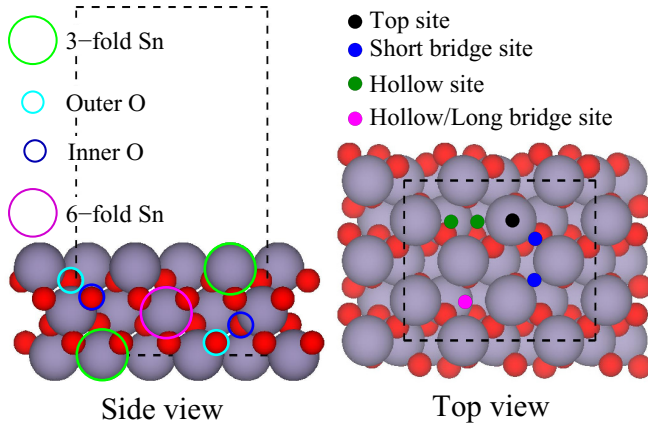


FIG. 1. Top and side view of the surface $\text{Sn}_3\text{O}_4(010)$ model using a 2×2 surface unit cell. The Sn and O atoms are indicated by gray and red spheres, respectively.

is Sn-terminated, i.e., we will not use any oxygen species pre-adsorbed on the surface, which can be important at O-rich environments [18,70]. The gas-phase molecules were modeled using a cubic box with 20 Å edge to avoid interactions among molecules from different image unit cells.

For total energy calculations for the molecule/ $\text{Sn}_3\text{O}_4(101)$ systems and additional calculations such as work function, Bader charge analysis, and electron density differences, we employed a $3 \times 2 \times 1$ \mathbf{k} -point mesh for the surface Brillouin zone (BZ) integrations, while larger \mathbf{k} -point mesh, $6 \times 4 \times 1$, was employed for density of states (DOS) calculations. For the gas-phase molecules, only the Γ point was considered as there is no dispersion in the electronic states. For the self-consistency of the electron density for all calculations, we employed a total energy convergence parameter of 10^{-6} eV, while the equilibrium structures were reached once the atomic forces on every atom were smaller than 0.01 eV/Å.

III. RESULTS AND DISCUSSIONS

Thus, employing the computational details described above, we performed a large number of calculations for the gas-phase molecules, clean surface, and for the adsorption of the selected molecules on $\text{Sn}_3\text{O}_4(101)(010)$, whose main geometric, energetic, and electronic results are summarized in Table I, II, and III. Below, we will discuss the most important

TABLE I. $\text{Sn}_3\text{O}_4(010)$ monolayer properties: average effective coordination number ECN_{av} , average weighted bond lengths d_{av} , and the effective Bader charge for each Sn and O atoms on different monolayer environments.

Atoms	ECN_{av} (NNN)	d_{av} (Å)	$Q_{\text{eff}}^{\text{B}}$ (e)
Sn ^{threefold}	3.00	2.12	1.28
Sn ^{sixfold}	6.00	2.09	2.44
O ^{outer}	3.13	2.12	-1.26
O ^{inner}	3.13	2.12	-1.24

TABLE II. Gas-phase properties for the selected molecules. Bond length d_0 , binding energy E_b , and angles. The deviations compared with experimental results [72] are given in percentage, e.g., $\Delta E_b = 100(E_b^{\text{DFT}} - E_b^{\text{Exp.}})/E_b^{\text{Exp.}}$ (1 eV \simeq 23.06 kcal mol⁻¹).

Molecule	d_0 (Å)	Δd_0 (%)	E_b (eV)	ΔE_b (%)	α (deg)
H ₂	0.75	1.6	-4.5	-4.4	
N ₂	1.11	0.8	-10.5	5.9	
O ₂	1.23	1.6	-6.2	17.1	
CO	1.14	1.1	-11.6	3.1	
NO	1.16	1.2	-7.4	11.2	
CO ₂	1.18	1.3	-17.9	6.0	180
NO ₂	1.21	1.5	-11.6		133.8
CH ₄	1.10	0.9	-18.2	0.1	109.5

results, while additional data and technical details can be found in Ref. [71].

A. Gas-phase molecules

The gas-phase properties for the studied molecules, such as binding energies, E_b , and bond length distances are summarized in Table II. The results are in agreement with previous experimental and theoretical results [52,72], i.e., the bond length and internal angles deviations are smaller than 1%, however, the binding energies show higher deviations, in which the worst case was observed for O₂ (17.1%), while for the remaining molecules were smaller than 12%. For the NO₂, there were no experimental results available, possibly due to the coexistence of phases below 140°C according to the equilibrium reaction $\text{N}_2\text{O}_4(\text{g}) \rightleftharpoons 2\text{NO}_2(\text{g})$ [73].

B. Clean surface properties

1. Geometric parameters

The Sn_3O_4 ML has a thickness of 5.33 Å and is formed by the stacking of Sn and O planes along the [010] direction, Fig. 1. To obtain an improved understanding of the Sn and O coordination numbers, we performed a structural analysis of the Sn_3O_4 slab using the effective coordination concept [74,75], which yields the effective coordination number in number of nearest neighbors (NNN) ECN_i , and weighted bond lengths d_{av}^i , for each atom within the unit cell i . In Table I, we report the average values for the chemical species with similar chemical environment. The Sn atoms located in the bottom and topmost layers of the Sn_3O_4 ML are threefold coordinated species, i.e., $\text{ECN}_{\text{av}} = 3$ NNN, with an average distance to the nearest O atoms of 2.12 Å, while within the layer, the Sn atoms are sixfold coordinated ($\text{ECN}_{\text{av}} = 6$ NNN) and $d_{\text{av}} = 2.09$ Å. In addition, once the Sn_3O_4 slab is Sn-terminated, all O atoms have almost the same coordination, $\text{ECN}_{\text{av}} \approx 3.13$ NNN, and $d_{\text{av}} = 2.12$ Å, with negligible differences between outer and inner O layers, Fig. 1.

2. Effective Bader charges

From Bader charge analysis [76], we obtained the effective Bader charge on each ion, $Q_{\text{eff}}^{\text{B}}$, in which $Q_{\text{eff}}^{\text{B}} = Z_{\text{val}} - Q^{\text{B}}$, where Z_{val} is the number of valence electrons and, Q^{B} , is the total Bader charge. Thus, $Q_{\text{eff}}^{\text{B}} > 0$ for cationic atoms

TABLE III. Geometric, energetic, and electronic properties for the molecule/Sn₃O₄(010) systems. Δd_0 is the bond length change upon adsorption; $\Delta\alpha$ is the molecule internal angle deviations after adsorption; $d_{\text{Mol-Surf}}$ is the center-to-center minimum distance between an atom from the molecule and the nearest surface atom (the atoms are indicated in parentheses); E_{ad} is the adsorption energy; $\text{VBM}^{\text{Mol/Sn}_3\text{O}_4(010)}$ is the VBM of the Molecule/Sn₃O₄(010) systems; $\text{VBM}^{\text{Sn}_3\text{O}_4(010)}$ is the VBM of the Sn₃O₄(010) substrate upon the adsorption of the molecular species; ΔVBM is the change of the substrate VBM upon adsorption with respect to the clean surface ($\text{VBM}^{\text{clean}} = 5.33$ eV), and $Q_{\text{eff}}^{\text{Bader}}$ is the effective Bader charge on the molecules. The reference vacuum level is set up as zero energy.

Molecule	Δd_0 (%)	$\Delta\alpha$ (%)	$d_{\text{Mol-Surf}}$ (Å)	E_{ad} (meV)	$\text{VBM}^{\text{Mol/Sn}_3\text{O}_4(010)}$ (eV)	$\text{VBM}^{\text{Sn}_3\text{O}_4(010)}$ (eV)	ΔVBM (eV)	$Q_{\text{eff}}^{\text{Bader}}$ (e)
H ₂	0.31	—	3.45 (H–Sn)	–64.2	–5.33	–5.32	0.01	–0.02
N ₂	0.06	—	3.79 (N–Sn)	–97.0	–5.32	–5.32	0.01	–0.03
O ₂	0.79	—	3.31 (O–Sn)	–138.1	–5.43	–5.43	–0.10	–0.12
CO	0.15	—	3.46 (C–Sn)	–137.5	–5.34	–5.34	–0.01	–0.05
NO	1.24	—	2.82 (N–Sn)	–278.8	–4.58	–5.52	–0.19	–0.23
CO ₂	0.02	–0.38	3.58 (O–Sn)	–166.9	–5.33	–5.33	0.00	–0.04
NO ₂	3.41	–11.33	2.46 (O–Sn)	–524.9	–5.33	–5.83	–0.50	–0.52
CH ₄	0.04	0.00	3.38 (H–Sn)	–118.3	–5.31	–5.31	0.02	–0.03

and $Q_{\text{eff}}^{\text{B}} < 0$ for anionic atoms. The results are summarized in Table I. The O anions within the Sn₃O₄ slab have nearly the same $Q_{\text{eff}}^{\text{B}}$, i.e., $-1.24 e$ (inner) and $-1.26 e$ (outermost), however, the same trend does not hold for the Sn cations, e.g., $Q_{\text{eff}}^{\text{B}} = 1.28 e$ (outermost) and $2.44 e$ (middle layer), suggesting the presence of two oxidation states of tin, namely Sn²⁺ (Sn threefold, bottom and topmost layer) and Sn⁴⁺ (Sn sixfold, middle layer), which can be confirmed as follows. Considering the system charge neutrality, we have (Sn²⁺)₂(Sn⁴⁺)(O²⁻)₄, in which 2 O come from outer layer and 2 from inner layer. Taking into account their effective Bader charge, we have $2 \times 1.28 + 2.44 + 2 \times [(-1.26) + (-1.24)] = 0$, holding the charge neutrality.

3. Local density of states

In Fig. 2, we show the local density of states (LDOS) for both the Sn₃O₄ bulk and Sn₃O₄ ML systems. For the bulk system, we can see a large contribution from O *p* states, for both valence (occupied states) and conduction (empty states) bands, where they dominate the valence band. Near to the valence band maximum (VBM) and the conduction band minimum (CBM), we can observe an increased contribution from Sn *s* and Sn *p* states, in which the *s*-states come from the threefold Sn atoms (layer-layer interface). The threefold Sn atoms will contribute for both occupied and empty states through the *s* (and in less extent *p*) and *p* states, respectively [17,47].

Looking to the LDOS for the Sn₃O₄ ML, it is observed some small differences from the bulk, like a shift of the states, a slight sharpening of the band, and an increase of the band-gap, which is expected due to the electronic confinement. However, the dominance of states is similar, i.e., O *2p* states dominate the valence band, but with a decreased contribution to empty states; and *5s* and *5p* states have significant contribution near to VBM, and to the empty states as well. Interestingly, comparing the bulk and monolayer LDOS, it can be seen a state centered at about 1.5 eV in the bulk LDOS, while it vanishes for a monolayer. In Fig. S6 (Ref. [71]), this feature is better seen and we can identify this state as belonging to Sn^{threefold} atoms, which suggests that this energy

level is derived from the Sn–Sn lone pairs interaction between Sn₃O₄ ML, being absent in the monolayer case.

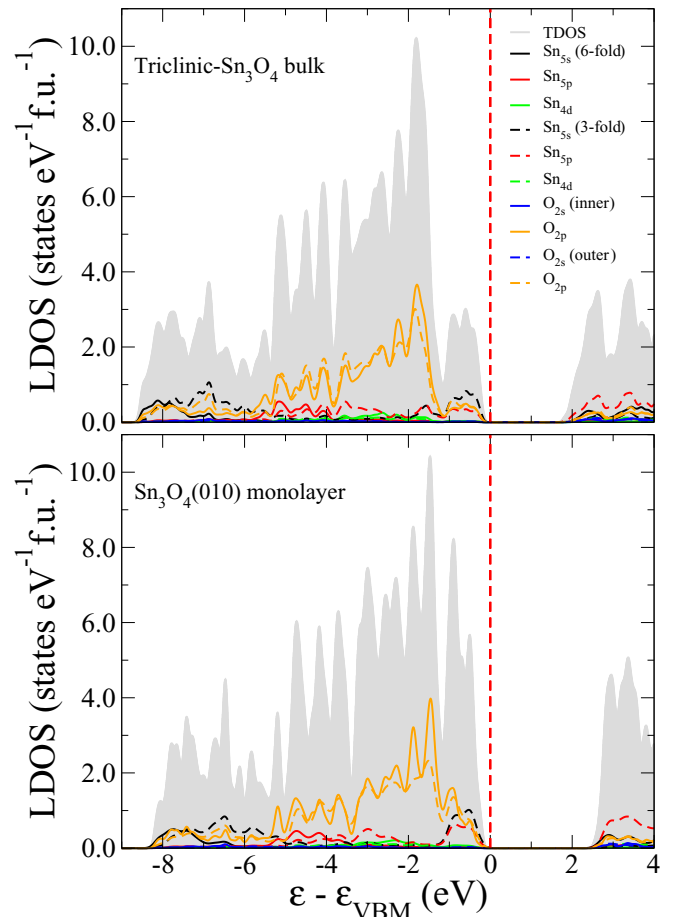


FIG. 2. Local density of states (LDOS) for the Sn₃O₄ bulk (top) and ML systems (bottom). Additionally, we separate the LDOS for Sn and O according with their coordination/location in the structure, as in Fig. 1.

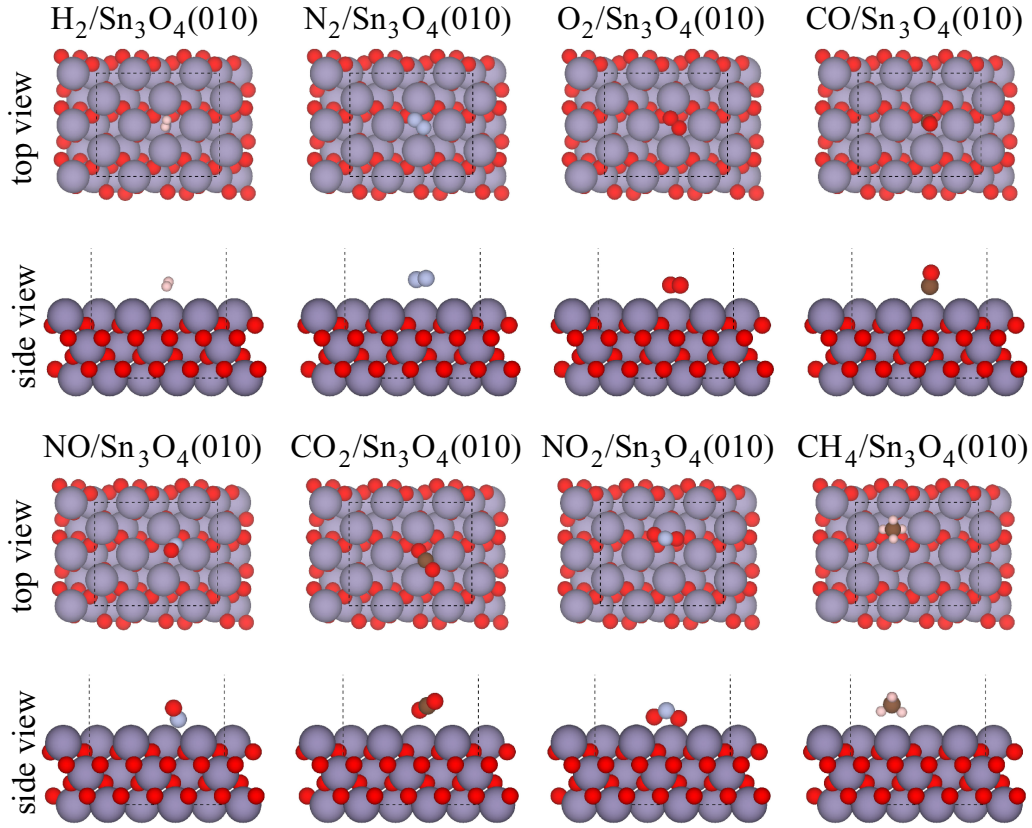


FIG. 3. Lowest energy configurations for H_2 , N_2 , O_2 , CO , NO , CO_2 , NO_2 , and CH_4 molecules adsorbed on the $\text{Sn}_3\text{O}_4(010)$ surface monolayer.

4. Surface energy and work function

Furthermore, we obtained a surface energy of $10.5 \text{ meV } \text{\AA}^{-2}$ [47], which is typical of van der Waals systems, and a work function of 5.33 eV by taking the Fermi level at VBM, i.e., $\Phi = V_{es}^{\text{vac}} - E_{\text{VBM}}$ [77,78]. At this study, work function changes will be used to obtain further information in the binding molecule-substrate mechanisms.

C. Adsorbed molecules on the $\text{Sn}_3\text{O}_4(010)$ surface

To obtain the lowest energy configurations for all molecule/ $\text{Sn}_3\text{O}_4(010)$ systems, we considered several adsorbed configurations according to the adsorption sites shown in Fig. 1, which were optimized using a local optimization algorithm. The lowest energy configurations are shown in Fig. 3, while the most important geometric, energetic, and electronic parameters are shown in Table III. All parameters are defined within the Ref. [71] along with comparisons between the lowest and higher energy adsorption configurations. Below, we will discuss the most important results.

1. Geometric parameters

The equilibrium distances between molecules and substrate are spread from 3.31 \AA (O_2) up to 3.79 \AA (N_2), except for NO_2 and NO , which approaches closer to the surface, i.e., 2.46 \AA (NO_2) and 2.82 \AA (NO). Thus, NO and NO_2 have higher bond lengths changes, Δd_0 , upon adsorption among all studied molecules, which reflects in the adsorption energies

E_{ad} results, i.e., larger magnitude for molecules closer to the surface. For several molecules, the Δd_0 increases as the E_{ad} increases in absolute value, except few cases. For example, for H_2 , Δd_0 is larger than for N_2 , but E_{ad} does not follow the same trend. A better relationship is observed for Δd_0 as a function of the molecule distance to the surface, $d_{\text{Mol-Surf}}$. In this case, Δd_0 increases as $d_{\text{Mol-Surf}}$ decreases. Thus, we can understand it as an increasing in the molecule-surface interaction. For N_2 , we found a larger $d_{\text{Mol-Surf}}$ (3.79 \AA) and, consequently, a smaller Δd_0 (0.06%). The CO_2 and CH_4 molecules presented a similar behavior.

2. Adsorption energies

The adsorption energies range from -64.2 meV (H_2) up to -524.9 meV (NO_2), and hence, we do not expect large changes in the substrate due to their small magnitudes. Based on those results, experimental trends can be discussed. For instance, the large E_{ad} magnitude for NO_2 can be related to the higher selectivity [49] of Sn_3O_4 NBs under detection of this molecule as observed experimentally by Suman *et al.* [19]. Similar theoretical results were previously obtained by Yao *et al.* [79] for SnO ML, in which the O_2 , NO and NO_2 molecules strongly adsorb on the SnO ML surface, with E_{ad} 's up to -1.69 , -0.46 , and -0.98 eV , respectively. In our cases, the E_{ad} 's are smaller, namely -138 , -279 , and -525 meV for O_2 , NO , and NO_2 , respectively. Furthermore, Yao *et al.* obtained the smallest molecule-ML distance for O_2 (2.066 \AA), followed by NO_2 and NO (around 2.5 \AA). We obtained the

following distances, 2.46, 2.82, and 3.31 Å for NO₂, NO, and O₂ molecules, respectively, which indicates favorable conditions for detection of NO₂ on Sn₃O₄ ML compared to O₂. Also, the smaller distances to the surface could be an indicative of chemisorption [80].

3. Electron density analyses

The total effective Bader charge, $Q_{\text{eff}}^{\text{Bader}}$, which is the sum of the effective Bader charges for the molecule's atoms, are summarized in Table III. We found a charge transfer from the material to the molecules, and the largest charge transfer is obtained for NO₂, $-0.52 e$, followed by NO and O₂, $-0.23 e$ and $-0.12 e$, respectively, while the magnitude is smaller than $0.05 e$ for the remaining molecules. As a consequence of the charge transfer from Sn₃O₄ to the molecules, we observed a shift towards lower energies of the substrate VBM, which affects the work function change upon adsorption.

At first, the electronegativity of the molecule species can play an important role on the effective Bader charge results. For all O-based hetero-atomic molecules, the O atom is anionic, as in gas phase systems, which in principle occurs because of its large electronegativity. The Pauling electronegativity of all species considered are 2.20, 2.55, 3.04, 3.44, and 1.96 for H, C, N, O, and Sn, respectively. Despite of the O₂ molecule is electrically neutral, the Pauling electronegativity difference between O–Sn is about 1.48. For CH₄, however, the electronegativity difference between C–Sn is much smaller, about 0.59. Thus the O–Sn interaction has a larger ionic character compared with the C–Sn interaction. Finally, in the case of CO₂, its larger $d_{\text{Mol-Surf}}$ influences on the decrease of the Bader effective charge despite of the O–Sn interaction. Thus, in this case the CO₂ molecule is almost not affected by the interaction with the surface as its conformation is not changed so much, $\Delta L = 0.02$, which also happens in the case of N₂. On the other hand, CO₂ activation could be facilitate on different Sn₃O₄ surface planes or in the presence of other species like H. For instance, Liu *et al.* obtained a great improvement of CO₂ reduction reaction by employing a hierarchical-Sn₃O₄ structure [81], in which the selectivity towards formate was increased compared with other reaction products like CO and H₂. Theoretically, they suggested that the Sn₃O₄(111) surface, combined with the presence of H species, favored the formation of OCHO* which is the intermediate of formate product, then supporting their experimental findings.

Yao *et al.* have pointed out that two different processes take place in the binding mechanism: covalent interactions of charge transfer and the dipole-dipole interactions due to polarization processes [79]: thus explaining why H₂ adsorbed on SnO has lower adsorption energy with a moderate charge transfer. Once most of molecules are in physisorbed-like state with zero dipole moment, the latter mechanism should be the dominant one for the H₂ [79]. However, the molecules with O atoms have an increased polarization interaction due to its higher electronegativity, contributing to increase the binding energy.

In Fig. 4, we show the isosurfaces of the electron density differences, $\Delta\rho$, upon the molecules-substrate interactions.

Additionally, in Fig. S7 in Ref. [71], we show the integration of electron density difference along z direction. In general, the region between the surface and molecule presented electron density accumulation and depletion, in which the accumulation is closer to the molecule, while the depletion to the surface. The electron density accumulation can be correlated with the effective charge transfer from surface to the molecule, as already discussed. In addition, the electron density depletion extending from the top surface to the vacuum region should contribute to an increase in the surface work function.

However, the isosurfaces cannot be directly comparable in most cases, once, as pointed in Fig. 4, their saturation levels are different. In this sense, the integration of electron density difference would be more helpful. Thus, according with Fig. S7 (Ref. [71]), H₂, N₂, and CH₄ were found to exhibit the smallest $|\Delta\rho| < 0.00025 e \text{ \AA}^{-3}$. Following, O₂, CO, and CO₂ with $|\Delta\rho| < 0.0016 e \text{ \AA}^{-3}$, then NO ($|\Delta\rho| < 0.006 e \text{ \AA}^{-3}$) and NO₂ ($|\Delta\rho| < 0.0075 e \text{ \AA}^{-3}$). Such different strengths indicate somehow the extent of interaction between the molecule and surface, once they can be related to the adsorption energy ranges.

The interaction of both NO₂ oxygen atoms through the same Sn site contributes to increase considerably its adsorption energy. Thus, a higher electron density accumulation can be observed in the molecule region, while a strong depletion region is observed right on the top of the Sn site. Again, this could be correlated with the larger charge transfer observed for NO₂. Furthermore, to accommodate both oxygen atoms above the Sn top site, the molecule is further distorted due to the size of the oxygen ions compared with the size of the Sn ions, and hence, it contributes to increase the magnitude of the interaction.

4. Effects of molecule adsorption on the electronic structure

The total density of states (TDOS) for all adsorbed systems is shown in Fig. 5. Just the systems with O₂, NO and NO₂ presented major changes in TDOS results. In these cases, the molecule-surface interaction are stronger, promoting a shift down in the states of the Sn and O atoms from the monolayer (less pronounced for O₂). For the other systems, the adsorbed molecules states just shift down compared to their gas-phase density of states (adsorptive molecule), generating an overlap between substrate and molecule states, in which the latter lies within the substrate valence and conduction bands, with no larger changes.

As observed, in most of cases the changes in the molecule states after interaction with the surface are small and there are no states within the band-gap of the surface states. However, for the O₂, NO, and NO₂ cases were observed molecule states within the gap. There are some distinct aspects relative to TDOS for the O₂, NO, and NO₂ molecules. These three cases presented magnetic moment, and the larger values of $Q_{\text{eff}}^{\text{Bader}}$. At experimental conditions, these new levels can be important once the charge transfer should increase, then populating them. Thus molecules will adsorb and a chemical bond will be formed with the surface. Afterwards, the molecule can hold adsorbed as an ion or dissociate to form other products. As mentioned by Yao *et al.* [79], these states can act as bridge

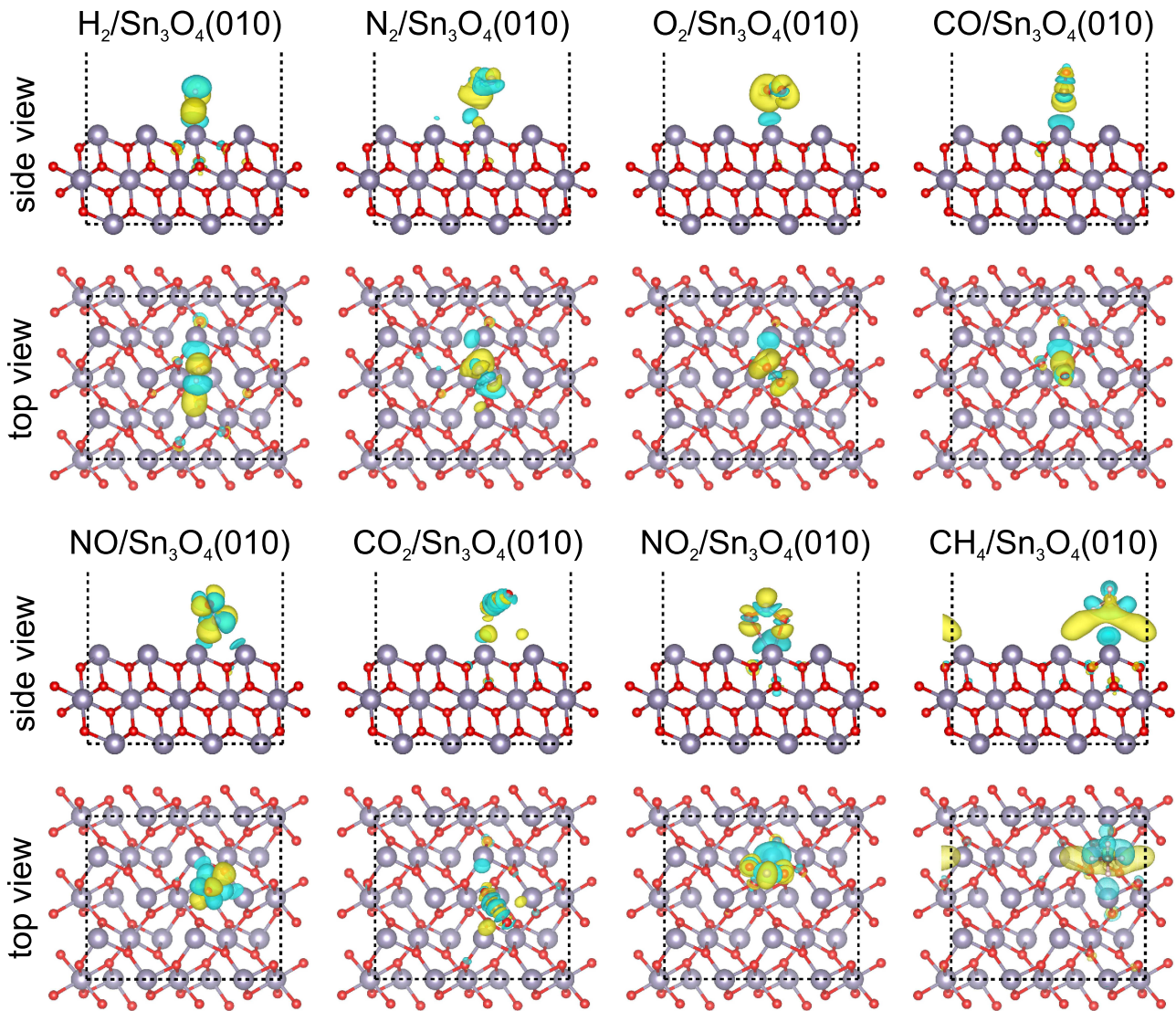


FIG. 4. Electron density differences upon the adsorption of molecules on the Sn_3O_4 monolayer. From left to right, side and top views for H_2 , N_2 , O_2 , CO , NO , CO_2 , NO_2 , and CH_4 , respectively. The yellow and cyan colors indicate increase and decrease of electron density, respectively. The isosurfaces are set to $0.0001 e \text{ \AA}^{-3}$ for H_2 , N_2 , and CH_4 ; $0.0005 e \text{ \AA}^{-3}$ for O_2 , CO , and CO_2 ; $0.002 e \text{ \AA}^{-3}$ for NO ; $0.003 e \text{ \AA}^{-3}$ for NO_2 .

states, reducing energy for electron transitions from VBM to CBM.

IV. EXPERIMENTAL INSIGHTS

Among all studied molecules, we found that NO and NO_2 have larger adsorption energies, which results in smaller distances to the substrate, as expected. Further, based on the electron density analysis, we identified a substantial charge transfer from the substrate to the molecules, in particular, to the NO_2 molecule due to the presence of two O atoms. As a consequence, we observed a shift towards lower energies of the substrate VBM, which is larger for NO_2 and smaller for NO due to the smaller magnitude of the charge transfer, such that we expect a strong contribution of the Coulombic interactions to the molecule-substrate binding. Despite of its moderate E_{ad} value, the O_2 molecule presented properties

similar to NO and NO_2 , namely, smaller $d_{\text{Mol-Surf}}$ and larger magnitudes for the charge transfer, $Q_{\text{eff}}^{\text{Bader}}$. On the other hand, different from NO and, particularly, NO_2 , the O_2 molecule does not tend to chemisorbs, but instead keep (iono)adsorbed through Coulombic interactions mostly thanks to its $Q_{\text{eff}}^{\text{Bader}}$.

Another common feature that O_2 , NO and NO_2 share is the presence of few states within the band gap, Fig. 5. If ionized, these states can trap electrons avoiding them to take part in the conduction process, favoring nonradiative recombination. For example, in a gas sensor device, such behavior could contribute to increase the resistance and consequently the sensor response given by the ratio between the resistances in presence of the targeted gas and the baseline resistance. Similar effects could occur for the NO_2 and the NO adsorption, being the difference that NO is a reducing gas at experimental conditions, and is expected to promote a decrease in the material resistance.

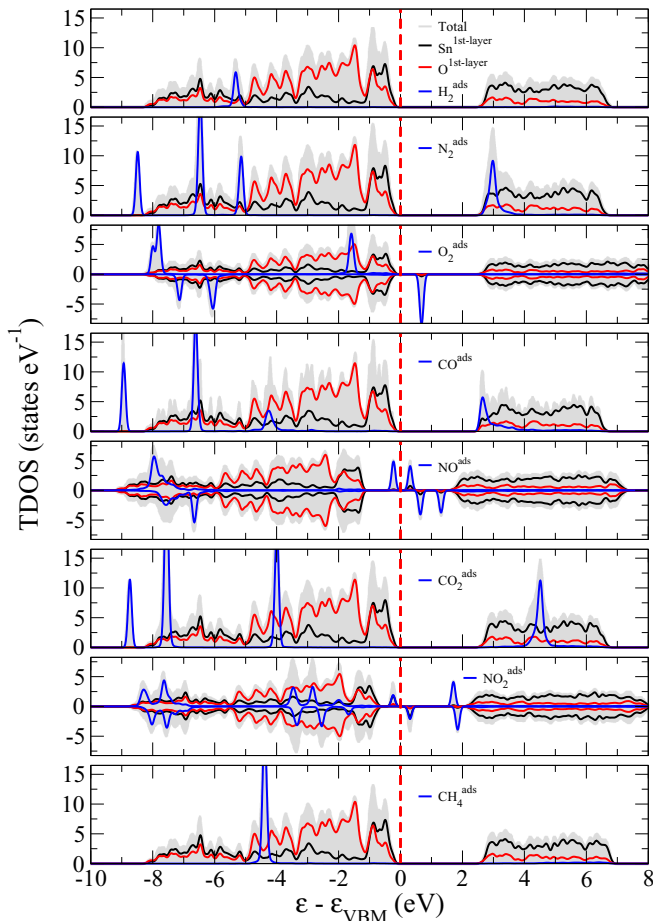


FIG. 5. Total and local density of states (TDOS, LDOS) for adsorbed systems: H_2 , N_2 , O_2 , CO , NO , CO_2 , NO_2 , and CH_4 . The LDOS of the first layers of Sn (black) and O (red) plus the adsorbed molecule (blue) were considered (gray). For the systems which present magnetic moment (O_2 , NO , and NO_2) the spin-up and -down contributions are considered.

It is worth noticing that in all cases there is a charge density accumulation near to the molecule region, Figs. 4 and S2 (Ref. [71]), which may induce a depletion region near to the surface, due to the molecule adsorption. At first, this depletion region could additionally contribute to increase the surface depletion layer, promoting an enhanced upward band bending [82], leading to the increase in resistance. Degler *et al.* showed a relationship between the band bending, ΔV_s , and the change in surface charge concentration, ΔQ_s , i.e., $\Delta V_s \propto \Delta Q_s$ [83]. Thus the extent of this effect could be seen through the effective charge transfer, once it seems that they present the same trend, i.e., $Q_{\text{eff}}^{\text{NO}_2} > Q_{\text{eff}}^{\text{NO}} > Q_{\text{eff}}^{\text{O}_2}$.

V. CONCLUSIONS

We have employed a spin-polarized DFT-PBE+D3 framework to study the adsorption properties of H_2 , O_2 , N_2 , CO , NO , CO_2 , NO_2 , and CH_4 on the $\text{Sn}_3\text{O}_4(010)$ monolayer. We observed that most molecules (H_2 , O_2 , N_2 , CO , CO_2 , CH_4) have a weaker adsorption energy, i.e., a feature of physisorption-like regime. However, NO and NO_2 have higher adsorption energies, -278.8 and -524.9 meV, in particular NO_2 , and smaller molecule-surface distances (2.82 and 2.46 Å) were obtained, respectively. Among all molecules, Sn_3O_4 ML was found to be more sensitive to O_2 , NO and NO_2 , which presented the larger charge transfers, $-0.12e$, $-0.23e$, and $-0.52e$, and a larger valence band maximum changes, 1.07 , 0.40 , and 1.16 eV, respectively. Their larger charge transfers give rise to higher electron density depletion near to the surface.

Despite the experimental exfoliation of Sn_3O_4 still challenging, theoretically Sn_3O_4 ML has a great potential for gas sensing applications toward the detection of O_2 , NO , and, particularly, NO_2 , for which an enhanced performance is suggested. Through our efforts to understand the molecules interaction with Sn_3O_4 ML, we expect not only contribute to future applications, as soon as the exfoliation of Sn_3O_4 made it possible, but also further understanding the adsorption processes at Sn_3O_4 surface, particularly as a gas sensor material. Additionally, our results could be very helpful in complement the scarce literature about Sn_3O_4 , either in its bulk or monolayer forms.

The data that support the findings of this study are available from the corresponding author upon reasonable request.

ACKNOWLEDGMENTS

We thank the Center for Scientific Computing (NCC/GridUNESP) of the São Paulo State University (UNESP) and QTNano Group by the computational resources provided. J.L.F.D.S. gratefully acknowledge support from FAPESP (São Paulo Research Foundation, Grants No. 2017/11631-2 and No. 2018/21401-7), Shell and the strategic importance of the support given by ANP (Brazil's National Oil, Natural Gas and Biofuels Agency) through the R&D levy regulation. M.O.O. acknowledges the financial support of FAPESP (Grant No. 2017/26219-0) and CNPq (National Council for Scientific and Technological Development, Grants No. 443138/2016-8 and No. 303542/2015-2). Furthermore, we thank the referees for their valuable suggestions, which helped to improve the manuscript.

- [1] M. Xu, T. Liang, M. Shi, and H. Chen, *Chem. Rev.* **113**, 3766 (2013).
- [2] G. R. Bhimanapati, Z. Lin, V. Meunier, Y. Jung, J. Cha, S. Das, D. Xiao, Y. Son, M. S. Strano, V. R. Cooper *et al.*, *ACS Nano* **9**, 11509 (2015).
- [3] K. S. Novoselov, A. Mishchenko, A. Carvalho, and A. H. Castro Neto, *Science* **353**, aac9439 (2016).

- [4] S. A. Tawfik, T. Gould, C. Stampfl, and M. J. Ford, *Phys. Rev. Mater.* **2**, 034005 (2018).
- [5] Z. Li, L. Yu, C. Milligan, T. Ma, L. Zhou, Y. Cui, Z. Qi, N. Libretto, B. Xu, J. Luo, E. Shi, Z. Wu, H. Xin, W. N. Delgass, J. T. Miller, and Y. Wu, *Nat. Commun.* **9**, 5258 (2018).
- [6] H. Tang, Q. Hu, M. Zheng, Y. Chi, X. Qin, H. Pang, and Q. Xu, *Prog. Nat. Sci.* **28**, 133 (2018).

- [7] Z. Lin, H. Shao, K. Xu, P.-L. Taberna, and P. Simon, *Trends Chem.* **2**, 654 (2020).
- [8] U. W. N. Barsan, in *Metal Oxide Gas Sensors*, edited by R. Moos (AMA Service GmbH, Nuremberg, Germany, 2012), pp. 618–621.
- [9] D. Hashoul and H. Haick, *Eur. Respir. Rev.* **28**, 1 (2019).
- [10] V. K. Ocampo-Restrepo, L. Zibordi-Besse, and J. L. F. Da Silva, *J. Chem. Phys.* **151**, 214301 (2019).
- [11] P. K. Kannan, D. J. Late, H. Morgan, and C. S. Rout, *Nanoscale* **7**, 13293 (2015).
- [12] S. Yang, C. Jiang, and S.-h. Wei, *Appl. Phys. Rev.* **4**, 021304 (2017).
- [13] F. Lawson, *Nature (London)* **215**, 955 (1967).
- [14] F. Gauzzi, B. Verdini, A. Maddalena, and G. Principi, *Inorganica Chimica Acta* **104**, 1 (1985).
- [15] A. Seko, A. Togo, F. Oba, and I. Tanaka, *Phys. Rev. Lett.* **100**, 045702 (2008).
- [16] J. Wang, N. Umezawa, and H. Hosono, *Adv. Energy Mater.* **6**, 1501190 (2016).
- [17] J. Savioli, A. L. Gavin, A. K. Lucid, and G. W. Watson, in *Tin Oxide Materials*, Metal Oxides, edited by M. O. Orlandi (Elsevier, Amsterdam, 2020), pp. 11–39.
- [18] N. Barsan, D. Koziej, and U. Weimar, *Sens. Actuator B-Chem.* **121**, 18 (2007).
- [19] P. Suman, A. Felix, H. Tuller, J. Varela, and M. Orlandi, *Sens. Actuator B-Chem.* **208**, 122 (2015).
- [20] M. Manikandan, T. Tanabe, P. Li, S. Ueda, G. V. Ramesh, R. Kodiyath, J. Wang, T. Hara, A. Dakshnamoorthy, S. Ishihara, K. Ariga, J. Ye, N. Umezawa, and H. Abe, *ACS Appl. Mater. Interfaces* **6**, 3790 (2014).
- [21] A. Huda, P. Suman, L. Torquato, B. F. Silva, C. Handoko, F. Gulo, M. Zanoni, and M. Orlandi, *J. Photochem. Photobiol. A-Chem.* **376**, 196 (2019).
- [22] R. Yang, Y. Ji, J. Zhang, R. Zhang, F. Liu, Y. Chen, L. Liang, S. Han, X. Yu, and H. Liu, *Catal. Today* **335**, 520 (2019), advances in photo(electro)catalysis for environmental applications and chemical synthesis.
- [23] M. Li, H. Zhu, G. Wei, A. He, and Y. Liu, *J. Mater. Sci. Mater. Electron.* **30**, 19625 (2019).
- [24] M. Batzill and U. Diebold, *Prog. Surf. Sci.* **79**, 47 (2005).
- [25] M. S. Barbosa, P. H. Suman, J. J. Kim, H. L. Tuller, J. A. Varela, and M. O. Orlandi, *Sens. Actuator B-Chem.* **239**, 253 (2017).
- [26] A. K. Singh, A. Janotti, M. Scheffler, and C. G. Van de Walle, *Phys. Rev. Lett.* **101**, 055502 (2008).
- [27] D. Ginley, H. Hosono, and D. Paine, *Handbook of Transparent Conductors* (Springer US, New York, 2010).
- [28] M. Singh, E. D. Gaspera, T. Ahmed, S. Walia, R. Ramanathan, J. van Embden, E. Mayes, and V. Bansal, *2D Mater.* **4**, 025110 (2017).
- [29] J. P. Allen, D. O. Scanlon, S. C. Parker, and G. W. Watson, *J. Phys. Chem. C* **115**, 19916 (2011).
- [30] *Oxide Semiconductors*, edited by B. Svensson, S. Pearton, and C. Jagadish, Semiconductors and Semimetals Vol. 88 (Academic Press, San Diego, CA, 2013), pp. 2–330.
- [31] M. O. Orlandi, A. José Ramirez, E. R. Leite, and E. Longo, *Cryst. Growth Des.* **8**, 1067 (2008).
- [32] H. Hosono, Y. Ogo, H. Yanagi, and T. Kamiya, *Electrochem. Solid State Lett.* **14**, H13 (2011).
- [33] P. Suman, A. Felix, H. Tuller, J. Varela, and M. Orlandi, *Sens. Actuator B-Chem.* **186**, 103 (2013).
- [34] K. Govaerts, B. Partoens, and D. Lamoen, *Solid Stat. Commun.* **243**, 36 (2016).
- [35] M. G. Masteghin and M. O. Orlandi, *Sensors* **18**, 3229 (2018).
- [36] J. B. Varley, A. Schleife, A. Janotti, and C. G. Van de Walle, *Appl. Phys. Lett.* **103**, 082118 (2013).
- [37] M. Batzill, *Sensors* **6**, 1345 (2006).
- [38] A. Martel, F. Caballero-Briones, P. Bartolo-Pérez, A. Iribarren, R. Castro-Rodríguez, A. Zapata-Navarro, and J. Peña, *Surf. Coat. Technol.* **148**, 103 (2001).
- [39] C. J. Damaschio, O. M. Berengue, D. G. Stroppa, R. A. Simon, A. J. Ramirez, W. H. Schreiner, A. J. Chiquito, and E. R. Leite, *J. Cryst. Growth* **312**, 2881 (2010).
- [40] O. M. Berengue, R. A. Simon, A. J. Chiquito, C. J. Dalmaschio, E. R. Leite, H. A. Guerreiro, and F. E. G. Guimarães, *J. Appl. Phys.* **107**, 033717 (2010).
- [41] P. H. Suman, E. Longo, J. A. Varela, and M. O. Orlandi, *J. Nanosci. Nanotechnol.* **14**, 6662 (2014).
- [42] S. Cahen, N. David, J. M. Fiorani, A. Maître, and M. Vilasi, *Thermochim. Acta* **403**, 275 (2003).
- [43] P. Sarker and M. N. Huda, *Comput. Mater. Sci.* **111**, 359 (2016).
- [44] Y. He, D. Li, J. Chen, Y. Shao, J. Xian, X. Zheng, and P. Wang, *RSC Adv.* **4**, 1266 (2014).
- [45] X. Li, F. Wang, J. Tu, H. U. Shah, J. Hu, Y. Li, Y. Lu, and M. Xu, *J. Nanomater.* **2015**, 980170 (2015).
- [46] K. Govaerts, R. Saniz, B. Partoens, and D. Lamoen, *Phys. Rev. B* **87**, 235210 (2013).
- [47] R. L. Freire, M. G. Masteghin, J. L. D. Silva, and M. O. Orlandi, *Comput. Mater. Sci.* **170**, 109160 (2019).
- [48] S. Grimme, *J. Comput. Chem.* **27**, 1787 (2006).
- [49] A. Oprea, D. Degler, N. Barsan, A. Hemeryck, and J. Rebbholz, in *Gas Sensors Based on Conducting Metal Oxides*, Metal Oxides, edited by N. Barsan and K. Schierbaum (Elsevier, Amsterdam, 2019), pp. 61–165.
- [50] P. Hohenberg and W. Kohn, *Phys. Rev.* **136**, B864 (1964).
- [51] W. Kohn and L. J. Sham, *Phys. Rev.* **140**, A1133 (1965).
- [52] J. P. Perdew, K. Burke, and M. Ernzerhof, *Phys. Rev. Lett.* **77**, 3865 (1996).
- [53] W. Liu, J. Carrasco, B. Santra, A. Michaelides, M. Scheffler, and A. Tkatchenko, *Phys. Rev. B* **86**, 245405 (2012).
- [54] P. Tereshchuk and J. L. F. Da Silva, *J. Phys. Chem. C* **116**, 24695 (2012).
- [55] J. Carrasco, J. Klimeš, and A. Michaelides, *J. Chem. Phys.* **138**, 024708 (2013).
- [56] R. L. H. Freire, D. Guedes-Sobrinho, A. Kiejna, and J. L. F. Da Silva, *J. Phys. Chem. C* **122**, 1577 (2018).
- [57] D. Guedes-Sobrinho, R. L. H. Freire, A. S. Chaves, and J. L. F. Da Silva, *J. Phys. Chem. C* **121**, 27721 (2017).
- [58] S. Grimme, J. Antony, S. Ehrlich, and H. Krieg, *J. Chem. Phys.* **132**, 154104 (2010).
- [59] S. Grimme, S. Ehrlich, and L. Goerigk, *J. Comput. Chem.* **32**, 1456 (2011).
- [60] W. Reckien, F. Janetzko, M. F. Peintinger, and T. Bredow, *J. Comput. Chem.* **33**, 2023 (2012).
- [61] G. Kresse and J. Hafner, *Phys. Rev. B* **48**, 13115 (1993).
- [62] G. Kresse and J. Furthmüller, *Phys. Rev. B* **54**, 11169 (1996).
- [63] J. Moellmann and S. Grimme, *Phys. Chem. Chem. Phys.* **12**, 8500 (2010).
- [64] S. Grimme, A. Hansen, J. G. Brandenburg, and C. Bannwarth, *Chem. Rev.* **116**, 5105 (2016).

- [65] B. M. Axilrod and E. Teller, *J. Chem. Phys.* **11**, 299 (1943).
- [66] Y. Muto, *J. Phys. Math. Soc. Jpn.* **17**, 629 (1943).
- [67] J. Moellmann and S. Grimme, *J. Phys. Chem. C* **118**, 7615 (2014).
- [68] P. E. Blöchl, *Phys. Rev. B* **50**, 17953 (1994).
- [69] G. Kresse and D. Joubert, *Phys. Rev. B* **59**, 1758 (1999).
- [70] P. H. Suman, *Sensores de gás a base de SnO₂-CuO*, Ph.D. thesis, Universidade Estadual Paulista, Araraquara, 2016.
- [71] See Supplemental Material at <http://link.aps.org/supplemental/10.1103/PhysRevMaterials.4.104002> for additional analyses of the local density of states of Sn₃O₄(010) surface divided according to the Sn and O atoms coordination contributions and the electron density difference integration along *z* direction.
- [72] W. M. Haynes, *CRC Handbook of Chemistry and Physics*, 94th ed. (Taylor and Francis, Boca Raton, 2013).
- [73] I. A. Leenson, *J. Chem. Educ.* **77**, 1652 (2000).
- [74] R. Hoppe, *Angew. Chem. Int. Ed.* **9**, 25 (1970).
- [75] J. L. F. Da Silva, *J. Appl. Phys.* **109**, 023502 (2011).
- [76] R. F. W. Bader, *Atoms in Molecules* (Oxford University Press, Oxford, 1990).
- [77] D. Cahen and A. Kahn, *Adv. Mater.* **15**, 271 (2003).
- [78] A. Kahn, *Mater. Horiz.* **3**, 7 (2016).
- [79] Y. Yao, Z. Li, T. Wang, K. Lu, P. Zhang, W. Zhang, and J. Yin, *Mater. Res. Express* **6**, 095078 (2019).
- [80] P. Atkins and J. de Paula, *Physical Chemistry*, 8th ed. (Oxford University Press, Great Britain, 2006) p. 1053.
- [81] L.-X. Liu, Y. Zhou, Y.-C. Chang, J.-R. Zhang, L.-P. Jiang, W. Zhu, and Y. Lin, *Nano Energy* **77**, 105296 (2020).
- [82] M. Hübner, R. Pavelko, N. Barsan, and U. Weimar, *Sens. Actuator B-Chem.* **154**, 264 (2011), EUROSENSORS XXIII.
- [83] D. Degler, U. Weimar, and N. Barsan, *ACS Sensors* **4**, 2228 (2019).